Natural Resources Research, Vol. 30, No. 1, February 2021 (© 2020)
https://doi.org/10.1007/s11053-020-09753-w

Original Paper

A Wavelet-Based Model for Determining Asphaltene Onset Pressure

Mohammad Heidary[1,2] and Kazem Fouladi Hossein Abad[1]

Received 29 July 2020; accepted 19 September 2020
Published online: 6 October 2020

Asphaltene onset pressure (AOP) is a significant parameter for determining the flow assurance of live oils. The solid detection system (SDS) is one of the prevalent techniques used by service laboratories to evaluate the stability of asphaltenes under reservoir conditions. The determination of AOP based on this technique entails the interpretation of recorded data, making the accuracy of the result prone to error. Accordingly, this research aimed to provide a robust computational method for determining AOP by wavelet analysis of SDS data. Changes in the curvature of transmitted light (CTL) were considered a diagnostic criterion to detect AOP. To substantiate this hypothesis, CTL was first calculated at each pressure. The discrete wavelet transform was then applied to decompose the CTL curve and compute the CTL entropy (E_{CTL}) based on the decomposition results. Finally, a relation was established between AOP and the entropy variations of CTL (ΔE_{CTL}), leading to the AOP determination model. This model indicated that the maximum value of ΔE_{CTL} is at AOP. Put differently, the onset of asphaltene precipitation pressure corresponds to the highest variation in the CTL entropy. The results obtained from the AOP determination model in various reservoirs are consistent with the experimental findings.

KEY WORDS: Asphaltene onset pressure, Solid detection system, Curvature of transmitted light, Entropy of transmitted light curvature, Discrete wavelet transform.

INTRODUCTION

One of the main factors that influence flow assurance during the primary production of oil reservoirs with main economic losses is precipitation and deposition of heavy organic components, especially asphaltene (Struchkov and Rogachev 2017). Asphaltene precipitation from live crude oils that occurs due to temperature or pressure reduction can lead to closure of flow paths within the reservoir rock (Mansourpoor et al. 2019; Kalantari and Farahbod 2019). In this regard, several studies have been conducted to investigate the impact of asphaltene deposition on reservoir rock properties. The findings show that porosity and permeability decrease dramatically as a result of asphaltene deposition (Memon et al. 2017; Mohammadzadeh et al. 2019; Ghadimi et al. 2019; Mehana et al. 2019; Qian et al. 2019). There is a wealth of evidence that rock wettability changes due to the adsorption of asphaltene and resin fractions on pore walls (Amin et al. 2011; Al-Aulaqi et al. 2011; Uetani 2014; Taqvi et al. 2016). Therefore, determination of the asphaltene onset pressure (AOP) at which asphaltene molecules first begin to precipitate out of solution is indispensable for managing the asphaltene threat.

The different understandings of the mechanisms behind asphaltene precipitation have led to the development of several theoretical and semi-

[1]Research Institute of Petroleum Industry (RIPI), Tehran, Iran.
[2]To whom correspondence should be addressed; e-mail: heidarym@hotmail.com

empirical models for predicting AOP (Nascimento et al. 2019; Esmaeili and Maaref 2018; Mahmoudvand et al. 2019; Abutaqiya et al. 2019). Various laboratory techniques have also been developed for determining AOP from live crude oil, including gravimetric, acoustic resonance, filtration, and solid detection system (SDS) (Pedersen et al. 2014). Despite being accurate, the gravimetric and filtration techniques are more time consuming than acoustic resonance and SDS techniques. The resonance changes detected by acoustic resonance technique are not unique to asphaltene precipitation, giving rise to potentially inaccurate onset measurements. The SDS technique using near-infrared light to probe fluids as asphaltene precipitates has gained broad acceptance within the petroleum industry.

Notwithstanding the reliability of the SDS technique in screening reservoir fluids for asphaltene, the interpretation of recorded data for an unambiguous determination of AOP is a daunting task. Accordingly, this study aimed to develop a rigorous computational method for determining AOP from SDS data. The entropy variations in the curvature of transmitted light (CTL) were considered a promising feature in detecting AOP. Calculation of the CTL entropy entails the extraction of CTL variations. The wavelet analysis, as a powerful information processing technique, can be used to decompose the CTL curve and to render CTL variations.

Over the last couple of decades, wavelets have found striking and wide applications in many branches of science and engineering. These applications include removal of electrical noise from signals, detection of abrupt discontinuities, and compression of large amounts of data. The results obtained from multiple investigations have shown that wavelets are an unrivaled choice for noise suppression and data compression (Xu et al. 2015; Dong and Ding 2016; Xie et al. 2017; Chen and Song 2018; Wang et al. 2020). The wavelet transform can viably capture abrupt changes and discontinuity in stationary and nonstationary signals (Heidary and Javaherian 2013; Heidary 2015; Wang and Zheng 2016; Kadkhodaie and Rezaee 2017; Zhang et al. 2018). Various researchers have presented wavelet-based solutions for detection and evaluation of hydrocarbon resources (Han et al. 2017; Naseer and Asim 2017; Heidary et al. 2019; Zhang et al. 2019; Azamipour et al. 2019).

This research aimed to test the robustness of the discrete wavelet transform (DWT) in detecting AOP based on SDS data. A model was derived based on the entropy variations of CTL to determine AOP accurately. The DWT coefficients, extracted from the CTL decomposition, were used to obtain entropy. The steps involved in this work are as follows: SDS data pre-processing, CTL calculation, decomposition of the CTL curve, entropy calculation, and derivation of the AOP model.

The most important advantage of the novel method over other existing methods is a solid foundation in theory and computation. The novel method furnishes a high temporal resolution of asphaltene precipitation not achievable in other methods, thereby rendering an accurate and reliable AOP. Moreover, the relative simplicity and quickness of computation make this novel method more useful and applicable in the determination of AOP compared to other methods.

MATERIALS AND METHODS

The proposed method for deriving the AOP determination model from the recorded data of the SDS technique comprises the following procedure.

1. Pre-processing was performed on SDS data. This step includes refining of SDS data, normalization of the refined SDS data, and smoothing of the normalized SDS data. In this regard, SDS data were first refined. This means that the different values of transmitted light power, recorded at a given pressure, were converted to a unique value by mathematical averaging. In addition, the recorded data were sorted by increasing (or decreasing) pressure. Then, the refined SDS data were normalized by a linear transformation. Finally, the normalized SDS data containing noise were smoothed by the DWT.
2. The pre-processed data were used to calculate CTL.
3. The DWT was applied to the CTL curve to extract detail (wavelet) coefficients. The detail coefficients are the result of the convolution of the CTL curve with the discrete wavelet coefficients. The detail coefficients served as a measure of the changes hidden in the CTL curve.
4. A parameter was provided for the description of the CTL disorder, referred to as the

CTL entropy. The CTL entropy was calculated based on detail coefficients.
5. The AOP determination model was derived from the variations of the CTL entropy.

Figure 1 illustrates the workflow of the above-described procedure. The proposed method was implemented in MATLAB software. The derived model was used to determine AOP in various reservoirs. The results obtained from this model were presented herein for five oil samples. Table 1 shows the composition of oil samples obtained from laboratory analysis.

Solid Detection System

The SDS technique detects AOP based on the scattering of laser light in a pressure–volume–temperature (PVT) cell. Light is scattered and it hardly passes through an oil sample owing to the formation of asphaltene particles. The onset pressure of asphaltene is determined by the interpretation of the light transmittance curve, which shows the amount of light received by a detector as a function of pressure during depressurization (or re-pressurization) process. Theoretically, the onset pressure of asphaltene precipitation in simple structured oils is determinable by a sudden change in the power of transmitted light (PTL). In effect, depending on the complexity of the oil structure, there are two or more turning points for most oil samples. The determination of AOP in complex oils based on the sudden change in PTL is virtually impossible. Accordingly, the SDS technique is ordinarily coupled with the filtration technique to obtain an accurate result from information analysis. Figure 2 schematically depicts SDS data with two turning points for an oil sample with an API gravity of 32°.

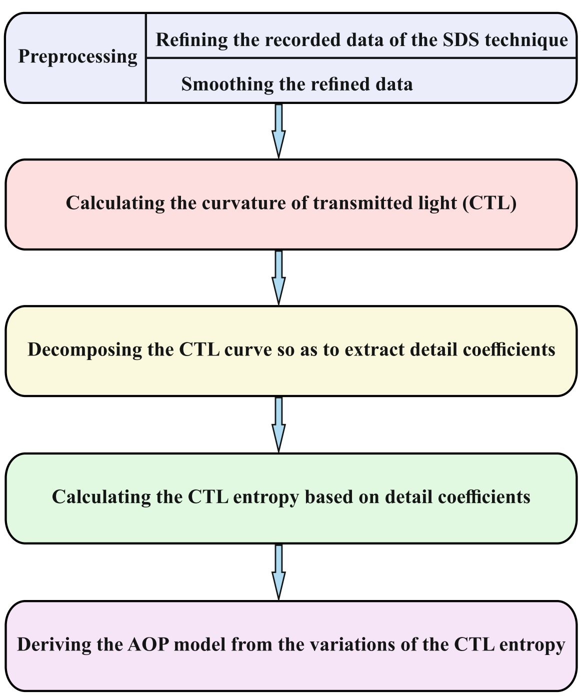

Figure 1. Workflow for deriving the AOP determination model from SDS data.

Given that the interpretation of the light transmittance curve for the AOP determination is inherently error-prone, especially when recorded data are distorted, this study intended to address this issue in a purely scientific sense. For this purpose, a dramatic change in CTL induced by asphaltene precipitation was postulated as a diagnostic criterion to detect AOP. The pre-processed SDS data were used to calculate CTL. Figures 3, 4, 5, 6 and 7 show the normalized light transmittance curve for the five samples under study. The curve of light transmittance was normalized using the min–max method to transform the SDS data into the range $[0, 1]$ (Berry et al. 2015):

$$S(P) = \frac{\mathrm{PTL}(P) - \min(\mathrm{PTL})}{\max(\mathrm{PTL}) - \min(\mathrm{PTL})}, \tag{1}$$

where $S(P)$ is the normalized PTL at a given pressure P. The onset pressure of asphaltene precipitation was obtained by the filtration technique. The experimental measurement of AOP is explained in the next section.

Filtration Technique

Filtration Setup

The experimental setup to conduct the asphaltene stability experiments is shown in Figure 8. The setup includes a high-purity CO_2 cylinder for CO_2 injection, a pressure regulator attached to the cylinder to control the pressure provided by the cylinder, and a filtration vessel. The filtration vessel contains crude oil, a rubber O-ring to prevent leakages during the experiment, a 0.2-μm polytetrafluoroethylene (PTFE) filter, and a 60-μm mesh screen used to support the filter membrane and prevent it

Table 1. Composition of oil samples under study

Component	Reservoir 1 (mol%)	Reservoir 2 (mol%)	Reservoir 3 (mol%)	Reservoir 4 (mol%)	Reservoir 5 (mol%)
H_2S	0.19	–	1.72	3.00	0.20
N_2	0.31	0.12	0.10	0.14	0.09
CO_2	5.88	2.02	3.37	5.20	2.40
C_1	25.4	43.59	44.01	25.12	48.32
C_2	7.54	9.47	8.92	9.90	8.83
C_3	4.82	5.49	5.41	7.50	5.12
iC_4	0.99	1.47	1.10	1.45	1.14
nC_4	2.39	3.06	3.03	4.40	2.92
iC_5	1.29	1.32	1.03	1.20	1.27
nC_5	1.3	1.53	1.14	1.02	1.35
C_6	10.67	5.19	3.31	4.47	4.77
C_7	4.53	3.89	3.50	3.81	3.49
C_8	3.5	2.96	1.37	3.54	2.47
C_9	4.24	4.27	2.54	2.70	3.41
C_{10}	3.1	2.81	1.93	2.45	2.70
C_{11}	2.45	2.83	1.85	2.10	2.93
C_{12}^+	21.4	10.00	15.66	22.00	8.59
$\gamma^a_{C_{12}^+}$	0.9867	0.8958	0.9137	0.9500	0.8997

[a] $\gamma_{C_{12}^+}$ is specific gravity of C_{12}^+

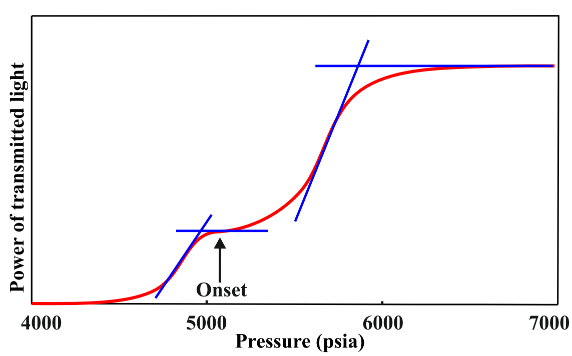

Figure 2. Power of transmitted light vs. pressure in the SDS technique [1 psia = ~ 6895 Pa].

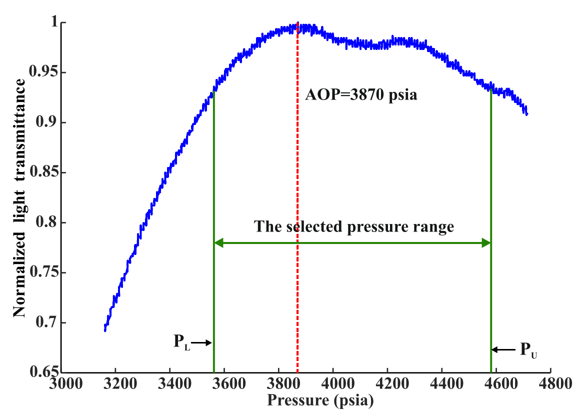

Figure 3. Normalized curve of light transmittance for oil sample of Reservoir No. 1 [1 psia = ~ 6895 Pa].

from being ruptured at high pressure. The produced oil, referred to as filtrate, is collected at the outlet in a glass test tube for further analysis (Fakher et al. 2019).

Determination of AOP

In this study, 100 ml of crude oil was poured into the filtration vessel. By injecting CO_2 into the vessel, the oil is passed through the filter membrane. The produced oil was gathered to determine the asphaltene weight percentage. Asphaltene extraction was implemented according to the IP-143 standard method. Then, 1 g of the filtrate was mixed well with 30 ml of the n-heptane solvent. The mixture was filtered through a 0.2-µm filter paper, and the resulting filter cake was washed thoroughly with additional n-heptane. All the extracted asphaltene on the filter paper was washed with toluene until the solvent became colorless. Finally, the precipitated asphaltene was oven-dried until the constant weight was achieved. The ratio of the asphaltene weight to the filtrate weight multiplied by 100 represents the asphaltene weight percentage. The asphaltene weight percentage with different CO_2 injection pressures was determined for the oil samples under study. Table 2, for example, displays the asphaltene weight percentage with different CO_2 injection pressures for the oil sample of Reservoir No. 4. At a

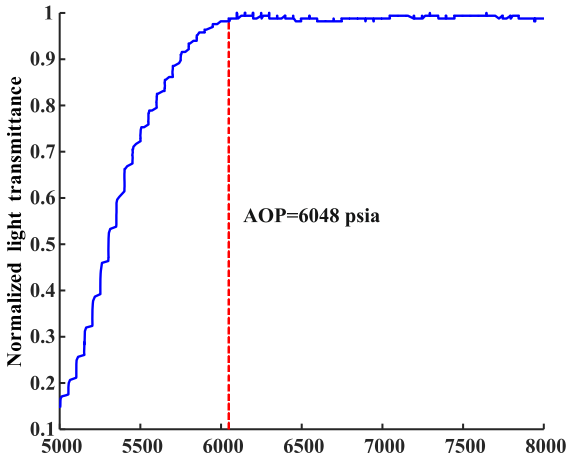

Figure 4. Normalized curve of light transmittance for oil sample of Reservoir No. 2 [1 psia = ~ 6895 Pa].

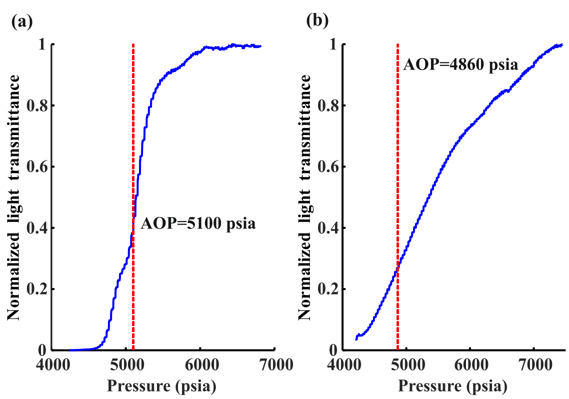

Figure 5. Normalized curve of light transmittance for oil sample of Reservoir No. 3: (**a**) depressurization process; (**b**) re-pressurization process. [1 psia = ~ 6895 Pa].

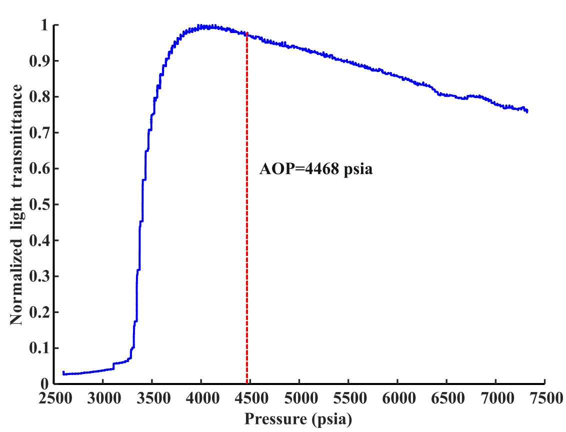

Figure 6. Normalized curve of light transmittance for oil sample of Reservoir No. 4 [1 psia = ~ 6895 Pa].

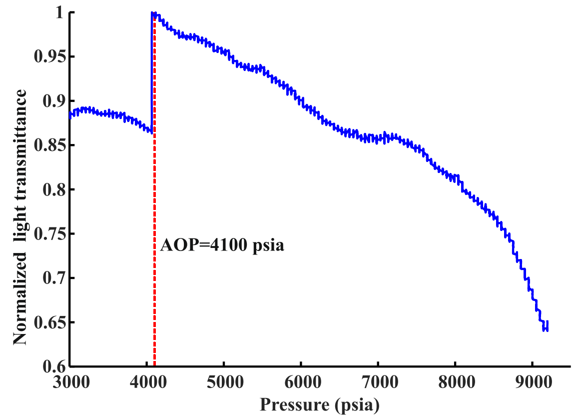

Figure 7. Normalized curve of light transmittance for oil sample of Reservoir No. 5 [1 psia = ~ 6895 Pa].

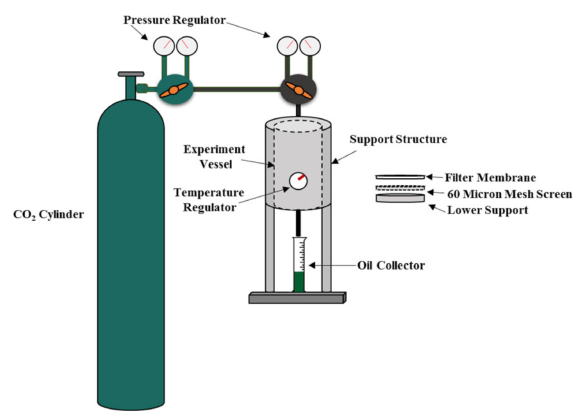

Figure 8. Schematic of filtration setup.

pressure of 7000 psia,[1] the asphaltene weight percentage was determined with and without a 0.2 μm filter membrane.

To determine AOP based on the results obtained from the filtrate analysis, first, the asphaltene weight percentage was plotted vs. pressure. Then, two lines were drawn between two consecutive points and intersected. The value of pressure at the intersection point is AOP. Figure 9, for example, depicts the determination of AOP in the oil sample of Reservoir No. 4. The asphaltene weight percentage corresponding to the pressure of 5500 psia was incorrect; thus, it was excluded. Table 3 exhibits the value of AOP obtained from the filtrate analysis for each reservoir under study.

[1] 1 psia = ~ 6895 Pa.

Table 2. Asphaltene weight percentage with different CO_2 injection pressures for oil sample of Reservoir No. 4

Pressure (psia[a])	Asphaltene weight percentage
7000	3.00 ← without filter
7000	2.83
5500	2.87
4000	2.72
2500	2.24

[a]1 psia = ~ 6895 Pa

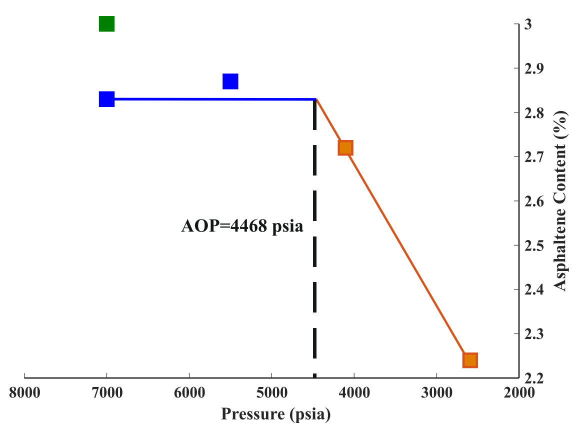

Figure 9. Determination of AOP in Reservoir No. 4 based on results obtained from filtrate analysis [1 psia = ~ 6895 Pa].

Table 3. Values of AOP obtained from filtrate analysis for each reservoir

Reservoir no.	AOP (psia[a])
1	3870
2	6048
3	5100 depressurization
3	4860 re-pressurization
4	4468
5	4100

[a]1 psia = ~ 6895 Pa

Curvature of Transmitted Light

The light passing through the oil sample has a specific curvature at each pressure. The curvature of transmitted light changes significantly at AOP as the homogeneous oil sample turns into two phases. The second derivative of the light transmittance curve provides a measure of CTL. Given the normalized SDS data (S), the CTL value at a given pressure (P) is calculated as (Mortimer 2013):

$$\mathrm{CTL}(P) = \frac{\frac{\mathrm{d}^2 S}{\mathrm{d}P^2}}{\left[1 + \left(\frac{\mathrm{d}S}{\mathrm{d}P}\right)^2\right]^{\frac{3}{2}}}. \qquad (2)$$

Because S is a discrete function, the first and second derivatives of S are calculated, respectively, as (Stoer and Bulirsch 2013):

$$\frac{\mathrm{d}S}{\mathrm{d}P} \simeq \frac{2S(P_{i+1}) - \frac{1}{2}S(P_{i+2}) - \frac{3}{2}S(P_i)}{h}, \qquad (3)$$

$$\frac{\mathrm{d}^2 S}{\mathrm{d}P^2} \simeq \frac{S(P_{i+2}) - 2S(P_{i+1}) + S(P_i)}{h^2}, \qquad (4)$$

where $S(P_i)$ is the normalized PTL at pressure ith (P_i) and $h = P_{i+1} - P_i$. The normalized SDS data must be free of noise to obtain accurate CTL. The DWT can effectively smooth the normalized SDS data.

Discrete Wavelet Transform

The wavelet transform is a method of converting a function (or signal) into another form, which either makes certain features of the original signal more amenable to study or enables the original data set to be described more succinctly. The kernel function of wavelet transform is defined as follows (Addison 2017):

$$\psi_{s,\tau}(t) = \frac{1}{\sqrt{s}}\psi\left(\frac{t-\tau}{s}\right), \quad s > 0, \tau \in R \qquad (5)$$

where $\psi(t)$ is the mother wavelet, s and τ are the scale (level) and the shift parameters, respectively. Wavelet transform can be divided in two categories—continuous wavelet transform (CWT) and DWT. The CWT of a function, $f(t)$, is the result of its inner product with the wavelet function (Gao and Yan 2010), thus:

$$\mathrm{CWT}(s,\tau) = \frac{1}{\sqrt{s}}\int_{-\infty}^{+\infty} f(t)\psi\left(\frac{t-\tau}{s}\right). \qquad (6)$$

In the DWT, the scale and shift parameters are discretized as: $s = 2^j$ and $\tau = k2^j$, with $j, k \in \mathbb{Z}$. The corresponding family of the base wavelet $\left(\psi_{j,k}\right)$ is expressed as:

$$\psi_{j,k}[n] = 2^{\frac{j}{2}}\psi\left(2^j n - k\right). \qquad (7)$$

The detail (or wavelet) coefficients $(d_{j,k})$ for signal $x[n]$ can be represented in terms of $\psi_{j,k}$, thus:

$$d_{j,k} = \sum_{n} x[n]\psi_{j,k}[n]. \tag{8}$$

Smoothing SDS Data

The data acquired with the SDS technique may be contaminated with noise, leading to an inaccurate value of AOP. Hence, noise suppression is an integral part of the process of deriving AOP from SDS data. The DWT can be employed to suppress noise, when necessary. Given N level of decomposition, the normalized curve of light transmittance, $S(n)$, is written as:

$$S(n) = D_1(n) + D_2(n) + \cdots D_N(n) + A_N(n), \tag{9}$$

where $D_i(n) = (d_1, d_2, \ldots, d_n)$ is the detail coefficients representing noise (or fluctuations) at level i and $A_N = (a_1, a_2, \ldots, a_n)$ is the smoothed $S(n)$. In practice, 1–3 decomposition levels are sufficient to smooth $S(n)$.

Curvature Entropy

From a physical point of view, the variation of CTL relative to pressure is negligible for a homogeneous oil sample. A remarkable shift in CTL occurs when asphaltene molecules initiate to precipitate out of solution. Accordingly, based on the variations of CTL, a parameter can be provided for the description of the CTL disorder. This parameter referred to as the CTL entropy (E_{CTL}) can distinctly highlight AOP. The approach adopted here to compute E_{CTL} from the C_{N} plot consists of the following five steps.

Step 1 During the SDS test, the pressure must be reduced gradually by 1 or 2 psi per second to ensure an accurate determination of AOP in the domain of the C_{N} plot. The sudden pressure drops (or fluctuations) accompanied by the sudden changes in C_{N} will result in detecting a pseudo-AOP. Hence, trimming the C_{N} plot is essential to exclude the misleading data, i.e., C_{N} values related to pressure fluctuations. In this regard, a pressure range $[P_{\mathrm{L}}, P_{\mathrm{U}}]$, was selected for each oil sample so that the upper pressure (P_{U}) was the beginning of the pressure fluctuations and the lower pressure (P_{L}) was before a perceptible increase in noise level. Accordingly, the domain of the C_{N} plot was trimmed by discarding the pressures lower than P_{L} and the pressures greater than P_{U}. In Figure 3, for example, the selected pressure range is shown.

Step 2 A small part of the trimmed C_{N} plot that is equivalent to a small pressure drop (or increase), e.g., $\Delta p = 30\,\text{psia}$, was separated from the end of the pressure range (or from the start of pressure range) and referred to as the kernel segment. Then, the kernel segment was decomposed by the DWT at the first level.

Step 3 Given the decomposition results of the kernel segment at resolution level 1, the maximum energy of the detail coefficients, $E_{\max}$, was determined as (Addison 2017):

$$E_{\max} = \max_{k}\left(d_k^2\right), \tag{10}$$

where d_k is the detail coefficient at location (pressure) k. The relative proportion of the total energy contained within $E_{\max}$ was then computed, referred to as E_n:

$$E_n = \frac{E_{\max}}{\sum_k d_k^2}. \tag{11}$$

Clearly, $\sum_k E_n(k) = 1$ and the distribution of E_n can be considered a pressure density at level 1. Entropy is a useful criterion for analyzing the complexity and probability distribution such as E_n, defined as:

$$E_{\mathrm{CTL}}^{(1)} = -E_n \ln(E_n), \tag{12}$$

where $E_{\mathrm{CTL}}^{(1)}$ represents the value of the CTL entropy in the first repetition. The corresponding pressure of $E_{\mathrm{CTL}}^{(1)}$ is $P_{\mathrm{U}} - \Delta p$ or $P_{\mathrm{L}} + \Delta p$ depending on where the kernel segment is separated; from the end of the interval (P_{U}) or from the start of the interval (P_{L}).

Step 4 The kernel segment was expanded by incorporating the first sample from the remaining part of the trimmed C_{N} plot. Steps 2 and 3 were then repeated, yielding the value of entropy in the second repetition, $E_{\mathrm{CTL}}^{(2)}$. This process was continued until the kernel segment turned into the trimmed C_{N} plot.

Step 5 Based on the CTL entropy, $E_{\mathrm{CTL}} = \left(E_{\mathrm{CTL}}^{(1)}, E_{\mathrm{CTL}}^{(2)}, \ldots E_{\mathrm{CTL}}^{(n)}\right)$, the variations of E_{CTL} was calculated as:

$$\Delta E_{\mathrm{CTL}}(P_i) = E_{\mathrm{CTL}}(P_{i+1}) - E_{\mathrm{CTL}}(P_{i-1}). \tag{13}$$

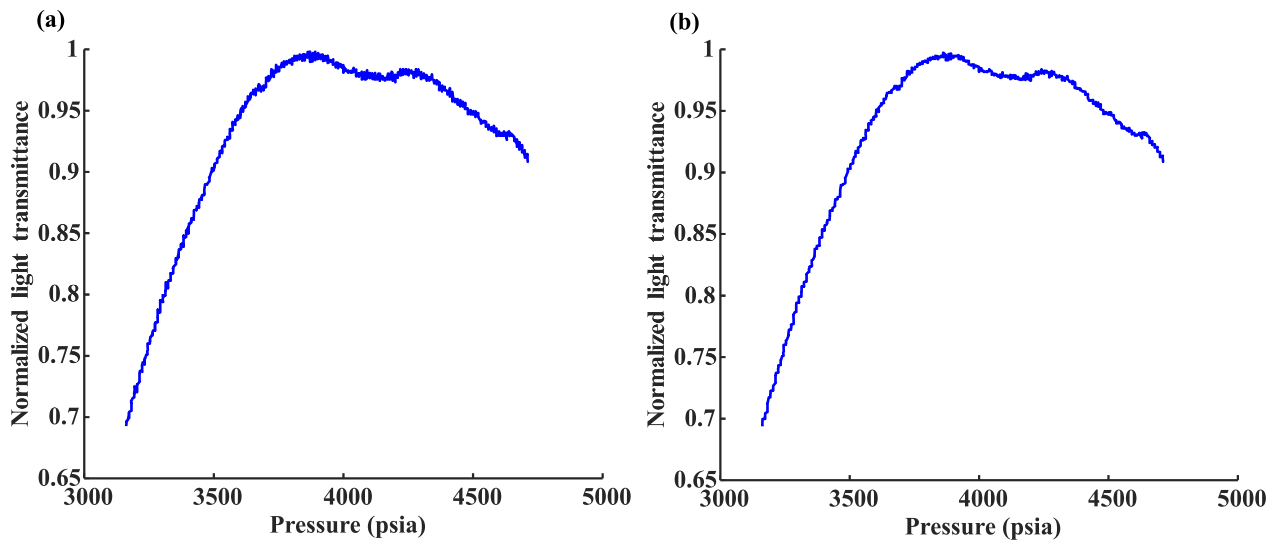

Figure 10. Smoothing of normalized light transmittance curve for oil sample of Reservoir No. 1: (**a**) $N = 1$; (**b**) $N = 2$ [1 psia = ~ 6895 Pa].

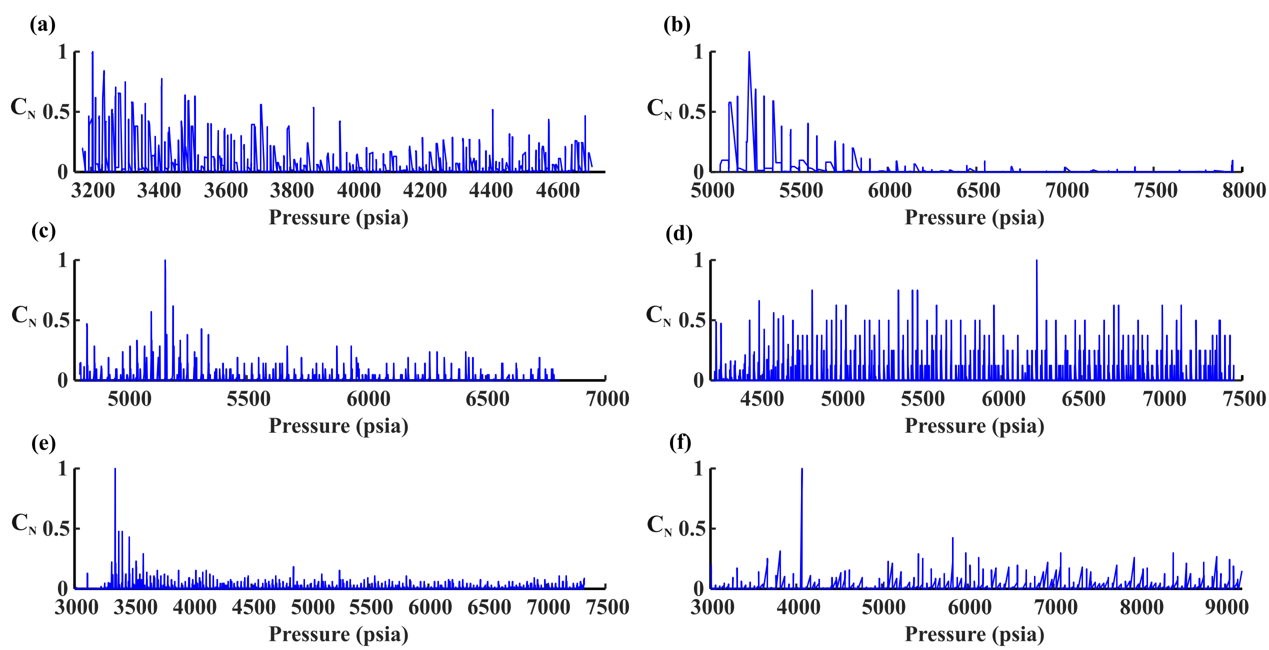

Figure 11. Absolute values of normalized CTL: (**a**) Reservoir No. 1; (**b**) Reservoir No. 2; (**c**) and (**d**) Reservoir No. 3; (**e**) Reservoir No. 4; (**f**) Reservoir No. 5. [1 psia = ~ 6895 Pa].

RESULTS AND DISCUSSION

The normalized SDS data were first smoothed by the DWT. Figure 10a and b, for example, shows the smoothing of the normalized light transmittance curve at levels 1 and 2, respectively, for the oil sample of Reservoir No. 1. The value of CTL at each pressure was then calculated. Figure 11 shows the absolute value of normalized CTL (C_N) vs. pressure for the studied samples. Figure 11c and d is related to the depressurization (Fig. 5a) and re-pressurization (Fig. 5b) process of the oil sample of Reservoir

Table 4. Values of AOP from wavelet-based and experimental methods for each reservoir

Reservoir no.	Wavelet type	AOP_T^a (psia[b])	AOP_M^a (psia)	$\Delta P = \lvert AOP_T - AOP_M \rvert$
1	Db2–Db3 Fk4–Fk6–Fk8 Bior5.5–Rbio5.5	3870	3881	11
2	Fk4 Bior (1.1–1.3–1.5) Rbio (1.1–1.3–1.5)	6048	6052	4
3	Db2–Db3 Bior (1.1–1.3–1.5) Rbio (1.1–1.3–1.5) Fk6	5100	5156	56
3	Db2 Sym4 Coif1–Coif2 Bior (1.3–1.5–2.2) Rbio (1.3–1.5–2.2)	4860	4823	37
4	Db2–Db3 Fk4 Bior1.1	4468	4440	28
5	All wavelets	4100	4067	33

[a] AOP_T and AOP_M stand for the AOP obtained by test and model, respectively
[b]1 psia = ~ 6895 Pa

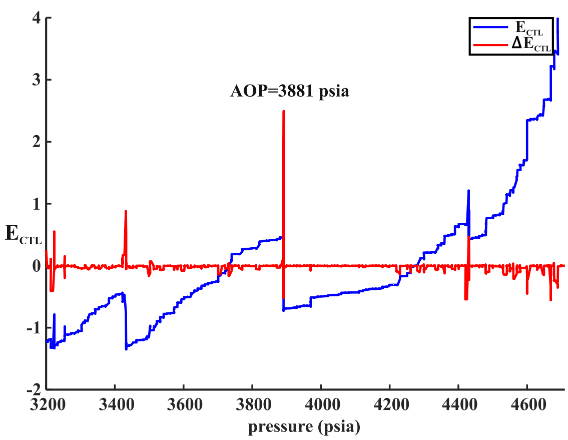

Figure 12. Values of E_{CTL} and ΔE_{CTL} vs. pressure for oil sample of Reservoir No. 1 [1 psia = ~ 6895 Pa].

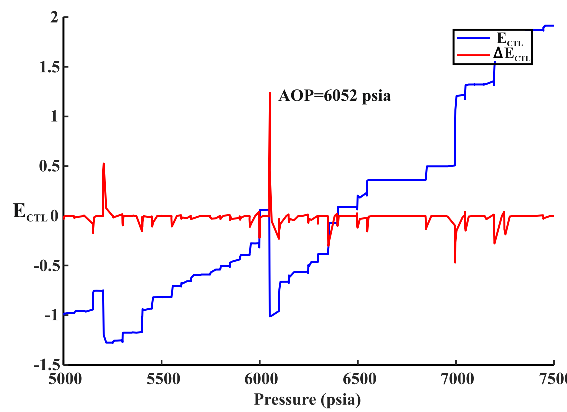

Figure 13. Values of E_{CTL} and ΔE_{CTL} vs. pressure for oil sample of Reservoir No. 2 [1 psia = ~ 6895 Pa].

No. 3, respectively. The C_N plot of the depressurization process is far removed from that of the repressurization process. This difference implies that asphaltene precipitation is irreversible.

Finally, values of E_{CTL} and ΔE_{CTL} at each pressure were calculated for the desired reservoirs. In this regard, various wavelets were used for calculating ΔE_{CTL} and thus detecting AOP. The results showed that only some wavelets could accurately detect AOP. Table 4 demonstrates which wavelets are capable of detecting AOP in each reservoir. Figures 12, 13, 14, 15 and 16 show the values of E_{CTL} and ΔE_{CTL} vs. pressure. The kernel segment was selected for the oil sample of Reservoir No. 3 and Reservoir No. 4 from P_L. The ΔE_{CTL} plot displays vividly the onset pressure of asphaltene corresponding to the maximum value of ΔE_{CTL}. Therefore, the AOP model is written as:

$$AOP = \max\{\Delta E_{CTL}(P_i) : P_i = P_1, \ldots P_n\}. \quad (14)$$

Equation (14) shows at what pressure the value of ΔE_{CTL} is maximum.

Trimming the domain of the C_N plot and selecting the kernel segment are pre-requisites for

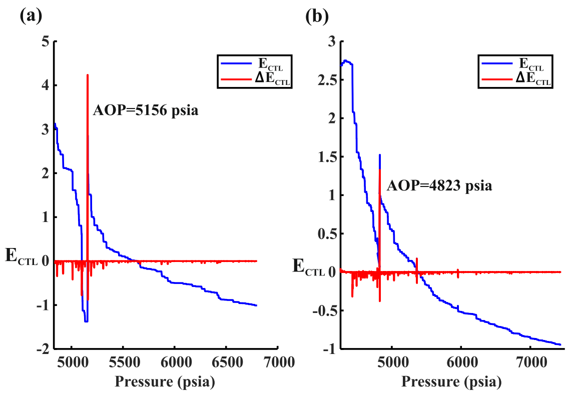

Figure 14. Values of E_{CTL} and ΔE_{CTL} vs. pressure for oil sample of Reservoir No. 3: (**a**) depressurization process; (**b**) re-pressurization process [1 psia = ~ 6895 Pa].

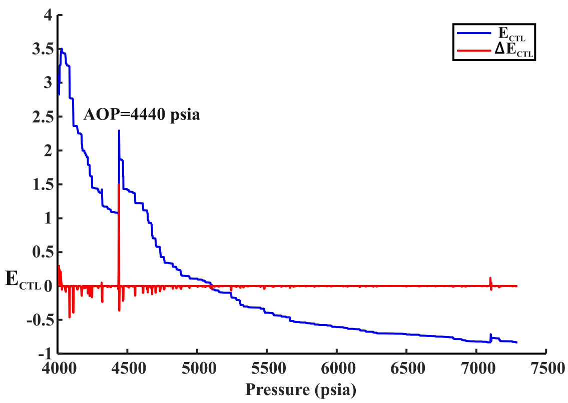

Figure 15. Values of E_{CTL} and ΔE_{CTL} vs. pressure for oil sample of Reservoir No. 4 [1 psia = ~ 6895 Pa].

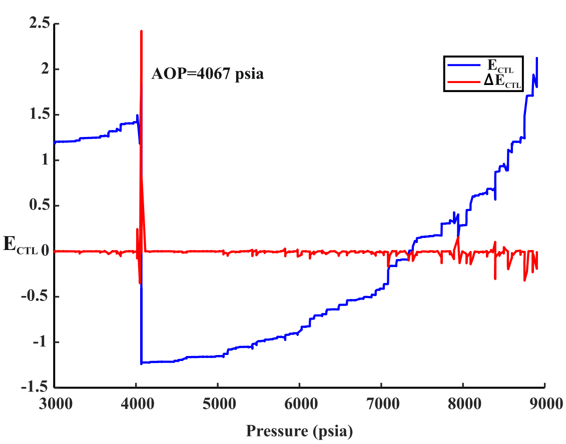

Figure 16. Values of E_{CTL} and ΔE_{CTL} vs. pressure for oil sample of Reservoir No. 5 [1 psia = ~ 6895 Pa].

computing ΔE_{CTL}. The former is required to highlight AOP accurately as well as to increase computation speed. A relatively large pressure drop with an incorrect value of PTL may be recorded during the test, leading to the appearance of a pseudo-AOP. Accordingly, by reducing the interval between P_L and P_U and consequently circumventing misleading records, AOP is accurately featured in the ΔE_{CTL} plot, provided that the turning points are within the interval. The latter is required to depict vividly ΔE_{CTL} vs. pressure. The kernel segment can be selected either from P_U or P_L, depending on the API gravity of the oil sample. It is recommended that the kernel segment be selected for oils with high API gravity (light oils) from P_U and for oils with low API gravity (heavy oils) from P_L.

CONCLUSIONS

The conceptual framework of the research was based on the remarkable change in CTL at the onset of asphaltene precipitation. In this regard, a model was developed that related AOP to the change in CTL entropy. To obtain such a model, the value of CTL was first calculated at each pressure. The DWT was then used to obtain ΔE_{CTL} at each pressure. Finally, the AOP model was determined based on ΔE_{CTL}. This robust model demonstrates that the maximum value of ΔE_{CTL} is at AOP. The results obtained from the AOP determination model in various reservoirs closely match the experimental findings, signifying that the remarkable change in light curvature at AOP is a tenable hypothesis. In this study, various discrete wavelets were utilized to determine the AOP model. Only the small-tap wavelets such as db2 were found to detect AOP at the highest resolution level accurately. Consequently, the dramatic change in CTL at AOP, which is visible only on a microscopic scale, is detectable with high-resolution wavelets.

ACKNOWLEDGMENTS

The authors gratefully acknowledge the support of the Research Institute of Petroleum Industry (RIPI) for this project.

REFERENCES

Abutaqiya, M. I., Sisco, C. J., & Vargas, F. M. (2019). A linear extrapolation of normalized cohesive energy (LENCE) for fast and accurate prediction of the asphaltene onset pressure. *Fluid Phase Equilibria, 483,* 52–69.

Addison, P. S. (2017). *The illustrated wavelet transform handbook: Introductory theory and applications in science, engineering, medicine and finance* (2nd ed.). New York: CRC Press.

Al-Aulaqi, T., Grattoni, C., Fisher, Q., Musina, Z., & Al-Hinai, S. (2011). Effect of temperature, oil asphaltene content, and water salinity on wettability alteration. In *SPE/DGS Saudi Arabia section technical symposium and exhibition, 2011*. Society of Petroleum Engineers.

Amin, J. S., Nikooee, E., Ghatee, M., Ayatollahi, S., Alamdari, A., & Sedghamiz, T. (2011). Investigating the effect of different asphaltene structures on surface topography and wettability alteration. *Applied Surface Science, 257*(20), 8341–8349.

Azamipour, V., Misaghian, N., & Assareh, M. (2019). Multi-level optimization of reservoir scheduling using multi-resolution wavelet-based up-scaled models. *Natural Resources Research*, *29*, 2103–2125.

Berry, M. W., Mohamed, A. H., & Yap, B. W. (2015). Soft computing in data science. In: *First international conference, SCDS, 2015* (p. 74). Berlin: Springer.

Chen, W., & Song, H. (2018). Automatic noise attenuation based on clustering and empirical wavelet transform. *Journal of Applied Geophysics, 159,* 649–665.

Dong, W., & Ding, H. (2016). Full frequency de-noising method based on wavelet decomposition and noise-type detection. *Neurocomputing, 214,* 902–909.

Esmaeili, S., & Maaref, S. (2018). Applying the Patel-Teja EoS with regular solution theory to predict the onset of asphaltene precipitation. *Fluid Phase Equilibria, 473,* 112–126.

Fakher, S., Ahdaya, M., Elturki, M., Imqam, A., & Elgahawy, Y. (2019) The effect of unconventional oil reservoirs' nano pore size on the stability of asphaltene during carbon dioxide injection. In *Carbon management technology conference, 2019*. Carbon Management Technology Conference.

Gao, R. X., & Yan, R. (2010). *Wavelets: Theory and applications for manufacturing*. Berlin: Springer.

Ghadimi, M., Amani, M. J., Ghaedi, M., & Malayeri, M. R. (2019). Modeling of formation damage due to asphaltene deposition in near wellbore region using a cylindrical compositional simulator. *Journal of Petroleum Science and Engineering, 173,* 630–639.

Han, X., Huang, Z.-X., Chen, X.-D., Li, Q.-F., Xu, K.-X., & Chen, D. (2017). On-line multi-component analysis of gases for mud logging industry using data driven Raman spectroscopy. *Fuel, 207,* 146–153.

Heidary, M. (2015). The use of kernel principal component analysis and discrete wavelet transform to determine the gas and oil interface. *Journal of Geophysics and Engineering, 12*(3), 386–399.

Heidary, M., & Javaherian, A. (2013). Wavelet analysis in determination of reservoir fluid contacts. *Computers & Geosciences, 52,* 60–67.

Heidary, M., Kazemzadeh, E., Moradzadeh, A., & Bagheri, A. M. (2019). Improved identification of pay zones in complex environments through wavelet analysis on nuclear magnetic resonance log data. *Journal of Petroleum Science and Engineering, 172,* 465–476.

Kadkhodaie, A., & Rezaee, R. (2017). Intelligent sequence stratigraphy through a wavelet-based decomposition of well log data. *Journal of Natural Gas Science and Engineering, 40,* 38–50.

Kalantari, F., & Farahbod, F. (2019). Mixing of crude oil with organic ZnO nano-particles from rice bran to improve physical properties of crude oil: A novel agent for enhanced oil recovery. *Natural Resources Research, 28*(3), 1183–1196.

Mahmoudvand, S., Shahsavani, B., Parsaei, R., & Malayeri, M. R. (2019). Prediction of asphaltene precipitation upon injection of various gases at near-wellbore conditions: A simulation study using PC-SAFT EoS. *Oil & Gas Science and Technology-Revue d'IFP Energies nouvelles, 74,* 63.

Mansourpoor, M., Azin, R., Osfouri, S., Izadpanah, A. A., & Saboori, R. (2019). Experimental investigation of rheological behavior and wax deposition of waxy oil-disulfide oil systems. *Natural Resources Research, 28*(4), 1609–1617.

Mehana, M., Abraham, J., & Fahes, M. (2019). The impact of asphaltene deposition on fluid flow in sandstone. *Journal of Petroleum Science and Engineering, 174,* 676–681.

Memon, A., Borman, C., Mohammadzadeh, O., Garcia, M., Tristancho, D. J. R., & Ratulowski, J. (2017). Systematic evaluation of asphaltene formation damage of black oil reservoir fluid from Lake Maracaibo, Venezuela. *Fuel, 206,* 258–275.

Mohammadzadeh, O., Taylor, S. D., Eskin, D., & Ratulowski, J. (2019). Experimental investigation of asphaltene-induced formation damage caused by pressure depletion of live reservoir fluids in porous media. *SPE Journal*. https://doi.org/10.2118/187053-PA.

Mortimer, R. G. (2013). *Mathematics for physical chemistry* (4th ed.). New York: Academic Press.

Nascimento, F. P., Souza, M. M., Costa, G. M., & Vieira de Melo, S. A. (2019). Modeling of the asphaltene onset pressure from few experimental data: A comparative evaluation of the Hirschberg method and the cubic-plus-association equation of state. *Energy & Fuels*, *33*(5), 3733–3742.

Naseer, M. T., & Asim, S. (2017). Detection of cretaceous incised-valley shale for resource play, Miano gas field, SW Pakistan: Spectral decomposition using continuous wavelet transform. *Journal of Asian Earth Sciences, 147,* 358–377.

Pedersen, K. S., Christensen, P. L., & Shaikh, J. A. (2014). *Phase behavior of petroleum reservoir fluids* (2nd ed.). New York: CRC Press.

Qian, K., Yang, S., Dou, H.-E., Pang, J., & Huang, Y. (2019). Formation damage due to asphaltene precipitation during CO2 flooding processes with NMR technique. *Oil & Gas Science and Technology-Revue d'IFP Energies nouvelles, 74,* 11.

Stoer, J., & Bulirsch, R. (2013). *Introduction to numerical analysis* (Vol. 12). Berlin: Springer.

Struchkov, I., & Rogachev, M. (2017). Risk of wax precipitation in oil well. *Natural Resources Research, 26*(1), 67–73.

Taqvi, S. T., Almansoori, A., & Bassioni, G. (2016). Understanding the role of asphaltene in wettability alteration using ζ potential measurements. *Energy & Fuels, 30*(3), 1927–1932.

Uetani, T. (2014). Wettability alteration by asphaltene deposition: A field example. In *Abu Dhabi international petroleum exhibition and conference, 2014*. Society of Petroleum Engineers.

Wang, F., & Zheng, S. (2016). Diagnostic of changes in reservoir properties from long-term transient pressure data with wavelet transform. *Journal of Petroleum Science and Engineering, 146,* 921–931.

Wang, P., Zhou, Y., Lv, Y., & Xiang, Y. (2020). Using wavelet filtering to perform seismometer azimuth calculation and data correction. *Computers & Geosciences*, *139*, 104447. https://doi.org/10.1016/j.cageo.2020.104447.

Xie, F., Xiao, C., Liu, R., & Zhang, L. (2017). Multi-threshold de-noising of electrical imaging logging data based on the wavelet packet transform. *Journal of Geophysics and Engineering, 14*(4), 900–908.

Xu, H., Sun, S. Z., Gui, Z., & Luo, S. (2015). Detection of sub-seismic fault footprint from signal-to-noise ratio based on wavelet modulus maximum in the tight reservoir. *Journal of Applied Geophysics, 114,* 259–262.

Zhang, F.-D., Liu, J., Lin, J., & Wang, Z.-H. (2019). Detection of oil yield from oil shale based on near-infrared spectroscopy combined with wavelet transform and least squares support vector machines. *Infrared Physics & Technology, 97,* 224–228.

Zhang, Q., Zhang, F., Liu, J., Wang, X., Chen, Q., Zhao, L., et al. (2018). A method for identifying the thin layer using the wavelet transform of density logging data. *Journal of Petroleum Science and Engineering, 160,* 433–441.